Structures of biomolecular complexes by combination of NMR and cryoEM methods

Philippe Cuniasse[1], Paulo Tavares[1], Elena V. Orlova[2] & Sophie Zinn-Justin[1,3#]

[1] *Institut de Biologie Intégrative de la Cellule (I2BC), CEA, CNRS, Univ. Paris Sud, Université Paris-Saclay, F-91198 Gif-sur-Yvette, France*

[2] *Institute of Structural and Molecular Biology, Birkbeck College, London WC1E 7HX, United Kingdom*

[3] *Institut de Biologie et de Technologies de Saclay, CEA, F-91191 Gif-sur-Yvette, France*

[#] *Corresponding author, sophie.zinn@cea.fr*

Short title: Combining cryoEM with liquid- and solid-state NMR

Abstract

CryoEM is presently providing structures of biocomplexes considered intractable to analysis by other structural techniques. NMR is playing an important role in delivering structural information on dynamics events and conformational heterogeneity. Impressive results were obtained by combining cryoEM and either liquid- or solid-state NMR, revealing the structures of cellular machines, filaments and amyloid fibrils. NMR solution structures of proteins and nucleic acids were fitted, together with crystallographic structures, into cryoEM maps of large complexes, to decipher their assembly mechanisms and describe their functional dynamics. Modeling based on solid-state NMR and cryoEM data provided 3D structure of filaments and fibrils. These NMR approaches validated, but also corrected, atomic models built *de novo* in cryoEM maps, and provided new structural data on flexible or structurally heterogeneous systems. Combination of cryoEM and NMR became an established hybrid approach in structural biology that significantly contributes to our understanding of functional mechanisms in supramolecular assemblies.

Highlights

- CryoEM combined with NMR provided atomic models of biocomplexes.
- NMR structures together with X-ray structures enabled interpretation of cryoEM maps.
- Solid-state NMR and cryoEM resolved structures of helical filaments and fibrils.
- These approaches validated and improved models built *de novo* using cryoEM maps.
- NMR structures were compared with cryoEM models to uncover assembly mechanisms.

Introduction

Understanding biological processes requires a detailed structure-function analysis of the supramolecular assemblies that build organisms, cells or viruses. Knowledge of the structures and dynamics of individual biological macromolecules forming these assemblies is essential to unravel function at the molecular level. Presently, X-ray crystallography, Nuclear Magnetic Resonance (NMR) spectroscopy, and cryo-electron microscopy (cryoEM) are the techniques that can deliver routinely high-resolution structures of macromolecules (Figure 1A,B). This review focuses on studies combining NMR and cryoEM in order to reveal the assembly mechanisms and dynamics of large biomolecular complexes (Figure 1C,D). We will illustrate the impact of the combination of these methods in solving challenging biological problems related to the function of large biomolecular systems.

X-ray crystallography solves a macromolecule structure if it can be trapped in a static conformation in a crystal. High-resolution structures ranging from small molecules to megadalton complexes were determined using this approach (Figure 1A,B). However, if some regions of a protein or a protein–nucleic acid complex are flexible, the diffraction pattern fades quickly and structural details are not observed in electron density maps. NMR provides information on an ensemble of structures reflecting different conformations in solution [1]. Structure determination using NMR spectroscopy is typically limited to proteins of less than 200 amino acids (Figure 1A,B). All segments of a protein or nucleic acid are found in the spectral representation of the structure, except in the case of specific millisecond timescale conformational exchange processes. Ability to visualize disordered regions in NMR spectra provides important information on their local structure and dynamics, as well as on their binding properties [2].

CryoEM is a technique used for determination of 3D structures of large protein complexes (Figure 1A,B) and also of proteins as small as 93 kDa (see recently [3]) from individual images of the biological assemblies. Computational methods offer the possibility to process populations of assemblies in different conformational states in a single preparation and to determine their independent structures [4,5]. During the last decade, technical advances and methodological developments have established cryoEM as a tool providing high resolution (often close to 3.5 Å) structures of macromolecules allowing *ab initio* building of atomic models (Figure 1C) [6-13]. Still, EM maps at a resolution of 5-10 Å constitute a large fraction of the recently reported results. In such cases, structures obtained by X-ray crystallography and NMR spectroscopy are used for rigid or flexible fitting to build pseudo-atomic models (Figure 1C) [14,15]. Rigid body fitting assumes that no conformational change takes place in the macromolecule structure at the resolution of the cryoEM reconstruction. Flexible fitting is used when conformational changes are detected in the macromolecular complex and positions of the known atomic model secondary elements (and sometimes loops) are adjusted to the EM densities to account for those changes.

Fitting of NMR atomic models into cryoEM structures of cellular machines

Historically, NMR has first provided ribosomal protein and RNA structures that were fitted into cryoEM maps of ribosomal complexes (light green bars in Figure 1D include several ribosomal subunit models) [16-18]. The inherent flexibility of RNA molecules renders their structural analysis by crystallography challenging, while they remain, if their size is not excessive, suitable targets for solution-state NMR-based approaches. Structures of RNA were also used to build a model of the human 80S ribosome in complex with hepatitis C virus internal ribosome entry site RNA [19,20] in

cryoEM maps at ~4-15 Å resolution. Recently, RNA solution structures combined with subunit X-ray structures contributed to the description of the *Tetrahymena* telomerase holoenzyme function based on a ~9 Å cryoEM map [21]. This model includes the telomerase reverse transcriptase, the integral telomerase RNA with its pseudoknot domain fragment showing a sequence complementarity with telomere repeats, a protein binding to telomeric DNA and several additional proteins. It revealed the path of the integral telomerase RNA in the enzyme catalytic core and the location of the telomeric DNA binding site.

More generally, NMR solution structures of numerous proteins with less than 180 amino acids were fitted, together with crystallographic structures of other proteins, into cryoEM maps of large complexes (light green bars in Figure 1D also include these models). Protein components were identified using this approach in the bacterial replicative DNA polymerase complex [22] and in the lid sub-complex of the yeast 26S proteasome [23,24]. In the latter study, the solution structures of the N-terminal and C-terminal domains of yeast Rpn9 validated but also corrected models built *de novo* in a 7.4 Å resolution cryoEM map (Figure 2A) [23]. These NMR structures were then fitted into the 3.5 Å 26S proteasome lid map, revealing the overall structural reorganization of the lid sub-complex during proteasome assembly [24].

In other studies, the NMR structures of small protein ligands were docked into large complexes obtained by cryoEM. A mammalian auxilin 1 fragment was localized in the clathrin lattice [25], doublecortin was identified on a microtubule surface [26], cofilin was positioned onto an actin filament [27] and the inhibitor Emi1 was localised in the human anaphase-promoting complex (APC/C) that controls chromosome segregation and mitotic exit [28,29]. In the study of the human cofilin/actin complex, a flexible fitting procedure was used to position the crystal structure of the actin monomer and the solution structure of cofilin arranged according to an experimentally determined helical symmetry within the filament 9 Å cryoEM map (Figure 2B). The resulting model revealed that rotation of the outer domain of actin upon cofilin binding alters the longitudinal contacts between actin protomers, highlighting the structural plasticity of actin filaments [27]. In the study of the E3 ubiquitin ligase APC/C complexed with the inhibitor Emi1, crystal structures together with homology models, were used to build most large APC/C subunits [29]. NMR ^{1}H-^{15}N heteronuclear nOe and Cα chemical shift dispersion analysis provided the delimitation of the structured zinc-binding region of Emi1 [28]. The resulting solution structure (Figure 2C) was localised within the low resolution negative-stain EM map of the APC/C-Emi1 complex. In order to position the Emi1 flexible regions, chimeric proteins were produced where two flexible regions of Emi1 were sequentially replaced by the globular β-propeller domain from yeast Doa1. The new regions of density observed in cryoEM maps served as markers for disordered regions. The globular and flexible domains of Emi1 were later fitted into a 3.6 Å resolution cryoEM map of the APC/C-Cdh1-Emi1 complex (Figure 2C). Analysis of Emi1 interaction with APC/C suggested a mechanism of inhibition of the E2s UbcH10 and Ube2S, which are responsible for catalysing ubiquitin chain initiation and elongation, respectively [29].

Structure determination by NMR and cryoEM of self-assembled filaments and amyloid fibers

Liquid-state NMR structures were also used to interpret the whole cryoEM map of self-assembled filaments and fibrils (dark green bars in Figure 1D). Fitting these structures into cryoEM maps yielded atomic models of the assembled complex and revealed conformational changes

associated to polymerization of monomers into filaments. The PB1 domain of the human autophagy receptor p62, involved in protein turnover and signaling, forms flexible helical polymers [30]. The NMR structure of the PB1 domain of rat p62 was fitted into the electron density of the PB1 helical scaffold determined at a resolution of ~10 Å (Figure 3A) [30]. The fitted PB1 molecules showed a dimer interface consistent with biochemical and structural data obtained on homologous PB1 domains. The resulting model explained how the C-terminal extension that is unfolded in monomeric PB1 also participates in filament assembly (Figure 3A).

Apoptosis-associated speck-like protein containing a CARD (ASC) is a component of mammalian inflammasomes that self-assembles to elicit host defense inside cells. Filaments consisting of pyrin domains of human ASC were characterized combining NMR and cryoEM [31]. The NMR structure of the ASC pyrin domain was modified in loop α2-α3 and in the short α3 helix for fitting into the 3.8 Å cryoEM density (Figure 3B) [31]. The fold of the pyrin domains of NLRP3 and ASC2 is similar to that of the ASC pyrin domain in filaments, suggesting that heteromeric filaments could be assembled during the formation of ASC-dependent inflammasomes.

Solid-state NMR is a technique for structure determination that is not limited by the size of the macromolecular assembly and has delivered structural information on complete protein filaments. Analysis of assigned chemical shifts led to determination of protein secondary structure while nOe measurements provided 3D short range proximities, either within a subunit or between different subunits. Combination of these data with the cryoEM filament structure allowed building an atomic model of several filaments of major biological relevance (light blue bars in Figure 1D). Study of the *Shigella* type III secretion needle was the first example in which solid-state NMR and EM methods were combined [32]. A 7.7-Å cryo-EM density map defined the orientations of MxiH subunits and α-helices while solid-state NMR provided backbone dihedral angles and a large set of carbon-carbon distance restraints from proton-driven spin diffusion experiments. The resulting models were cross-validated using a second large set of carbon-carbon and hydrogen-hydrogen distance constraints obtained from CHHC and NHHC experiments. They showed that, in contrast to a published model determined using cryoEM data alone [33], the MxiH N-terminus is positioned on the surface of the needle while the C-terminus points towards the lumen (Figure 3C; also previously proposed in [34]). This study provided one of the best defined solid-state NMR structures reported to date.

Solid state NMR and cryoEM were also combined to solve the mammalian ASC inflammasome structure [35]. Solid-state NMR identified the mouse protein domain involved in filament assembly. Comparison of solution-state and solid-state NMR chemical shifts demonstrated that no major structural rearrangements occurred during filament formation and identified residues located at ACS subunit interfaces. A large set of dihedral angle and carbon-carbon distance restraints was combined with the cryoEM density map (solved at ~4 Å) to determine the 3D structure of the filament. The tertiary and quaternary structures of mouse and human ASC filaments demonstrated good agreement, suggesting functional conservation of the ASC polymerization mechanisms as part of the innate immune response system.

NMR and EM techniques enabled characterization of the mechanisms of amyloid fibril formation [36] and determination of the 3D structures of self-assembled fibrils. A large number of intramolecular distance and torsion angle restraints were measured by solid-state NMR in the cross-

β amyloid fibrils formed by an 11-residue peptide from transthyretin [37], resulting in a first 3D model of the peptide. To identify intermolecular restraints, samples with a single isotopically labelled carbonyl atom per molecule were prepared and ^{13}CO-^{13}CO proximities were observed. Furthermore, several ^{13}C,^{15}N-labelled analogues were produced in order to measure additional carbon-carbon and carbon-nitrogen distance restraints. From these solid-state NMR data combined with the cryoEM maps of the fibrils, atomic models of doublet, triplet and quadruplet structures of the transthyretin fibrils were calculated. These structures revealed details of the packing interactions responsible for hierarchical assembly of transthyretin into protofilaments, filaments and mature fibrils [37].

New approaches are now being developed that provide a description of the dynamics of protein assemblies from solid-state NMR data [38]. First results demonstrated that it is possible to estimate the amplitude of motions with a timescale shorter than 10 μs in mature amyloid β fibrils from the analysis of ^{1}H-^{13}C dipolar couplings, ^{13}C chemical shifts and linewidths [39]. Recently, a multi-timescale analysis of the backbone dynamics of the prion forming domain of the fungus HET-s protein assembled into fibrils was described based on R_1 and $R_{1\rho}$ data sets and REDOR measurements for most backbone ^{15}N and ^{13}Cα nuclei [40]. Experimental ^{15}N and ^{13}Cα data could be explained using a motion model including three timescales (about 100 ps, 100 ns and 10 μs), suggesting that solid-state NMR can describe local to global fibril motions. Using these approaches, it should be possible to combine cryoEM structural analyses of biomolecular complexes with a description of their dynamics at the atomic level by solid-state NMR.

Structures of viral particles

Large viral assemblies with high point group symmetry have been resolved at near atomic resolution by cryoEM [9,10]. When lower resolution cryoEM maps were available, NMR has largely contributed to achieve molecular details through determination of the solution structures of viral protein components followed by flexible fitting of these atomic models into the cryoEM electron densities. One example is the head-to-tail connector of tailed bacteriophages that regulates the viral DNA exit from the phage capsid. CryoEM maps were determined for the phage SPP1 connector in different states: alone and bound to tail proteins [41,42]. The SPP1 portal protein structure was defined by X-ray crystallography [43]. The structures of head and tail completion protein monomers, which assemble to form the connector-tail interface, were solved in solution by NMR (see gp16 in Figure 4A) revealing several highly flexible regions in their monomeric states [44,45]. Flexible fitting of the head and tail completion protein structures was done in the connector bound to the phage tail before (Figure 4D) and after DNA ejection [42]. The resulting pseudo-atomic models revealed conformational changes that occur during assembly of the viral particle. They suggested a mechanism for portal channel closure after DNA packaging in which loops of gp16 subunits fold to assemble an intersubunit parallel β-sheet that plugs the portal channel (Figure 4B,C) [42]. This is achieved by an allosteric mechanism [42]. The gp16 plug then opens at the beginning of infection for DNA release and re-closes afterwards [42].

Solution NMR data were also instrumental to understand the structural transition of the bacteriophage P22 procapsid to mature capsid. The main capsid protein from P22 has the characteristic HK97 fold of the tailed phages-herpesviruses lineage but includes an additional insertion domain (I-domain). 3D structures of the I-domain were initially modelled using 8.2 and then 3.8 Å resolution cryoEM maps. However, the NMR structure of the I-domain alone and its fitting into

the 3.8 Å EM map of the procapsid as well as in the 4.0 Å EM map of the mature virion provided more convincing structures of the I-domain in the P22 capsid protein [46]. Two loops are disordered in both the isolated I-domain and in the full-length capsid protein but become ordered when the capsid protein assembles into icosahedral particles. The D-loop is involved in intercapsomer stabilizing interactions in procapsids, whereas the S-loop makes intrasubunit contacts that are likely important for capsid size determination [46].

Solution and solid-state NMR data contributed to the description of the human immunodeficiency virus type 1 (HIV-1) capsid, which is composed of ~1500 copies of the capsid protein (CA). HIV-1 CA consists of two domains, an N-terminal domain (NTD) and a C-terminal domain (CTD), connected by a flexible linker. In solution, HIV-1 CA dimerization depends on several CTD residues. When studied alone the CTD monomers exhibit different relative orientations compared to previous CTD X-ray structures. Fitting of the CTD atomic model obtained by NMR into 16 Å [47] and 8 Å [48] cryoEM maps of helical HIV-1 CA assemblies revealed that the NMR dimer interface is consistent with the CTD/CTD interface in the capsid. The study of the Mason-Pfizer monkey virus Gag polyprotein comprising the CA domain provided a 8 Å electron density map of the immature retrovirus by combining cryoEM and tomography [49]. The NTD structure of this CA protein was solved by NMR [50] and fitted into the cryoEM map, together with the homologous HIV-1 CTD NMR structure. This model explained the role of the NTD and CTD domains in retrovirus assembly and maturation. The host cell factor cyclophilin A interacts directly with the HIV-1 capsid and regulates viral infectivity. In a study of cyclophilin A - HIV-1 capsid interaction, a cryo-EM map of the complex was obtained at 8.6 Å and solid-state NMR was used to identify residues of the binding interface in both partners. This was achieved by monitoring the ^{15}N and ^{13}C NMR chemical shift perturbations of both proteins upon binding [51]. Mechanisms of cyclophilin recruitment onto the capsid and HIV-1 capsid stabilization were derived from this study.

Conclusion

The recent achievements of cryoEM have attracted structural biologists from other fields. Indeed, cryoEM has generated a large number of structures of biocomplexes that were considered as unsuitable to analysis by other structural techniques. Its power to reach near-atomic resolution created a momentum on the structural biology of macromolecules larger than 80 kDa. CryoEM can, at present, rapidly provide structures of large biological assemblies in different functional states. NMR, on the other side, is a technique that excels at determining sets of atomic structures from small proteins, or protein domains, and at analysing the dynamics of their flexible regions in solution. As these polypeptides are often part of large biological complexes, NMR is instrumental at uncovering conformation changes or even folding events associated with assembly of the large complexes whose atomic structures were determined by cryoEM. NMR is also a unique approach to identify a distribution of conformers within a large molecular machine in solution [52]. By correlating the local structural heterogeneity observed by NMR and the different large scale rearrangements identified by cryoEM, it is possible to propose detailed pseudo-atomic models for these molecular machines in different conformational states. Solid-state NMR is another approach that is becoming increasingly important to provide structural constraints and build precise atomic models in cryoEM density maps of homopolymers. We expect to see in the near future further integration of NMR, X-ray cristallography, cryoEM and modeling hybrid methods combined with their progressive automation. They will not only deliver atomic structures of biological machines but will also establish

molecular movies enlightening how conformational changes in those machines achieve biological function.

Acknowledgments

The authors thank Prof A. Lange for fruitful discussions and Dr C. Sachse for providing the negative staining image of the p62 filament shown in Figure 3A. Institutional funding was provided to the authors by the French National Center for Scientific Research (CNRS; P.C., P.T. and S.Z.-J.) and the Alternative Energies and Atomic Energy Commission (CEA; P.C. and S.Z.-J.).

Legends

Figure 1. Statistical analysis of the 3D structures or models deposited in the PDB and EMDB databases, determined from NMR, X-ray crystallography, EM data, and from hybrid methods. (A, B) Distribution of the protein structures deposited at the PDB (version August 2016) as a function of **(A)** the number of residues per protein chain or **(B)** the oligomerisation state of the proteins (when indicated in the PDB). Results are normalized by the total number of proteins whose structure was analysed by each technique: NMR (10093 references), X-ray crystallography (101785 references), EM (802 references). **(C, D)** Distribution of the number of publications describing models built from NMR and EM data as a function of **(C)** the resolution of the EM map or **(D)** the methodological approach used to calculate the model. Articles reporting a structural study linked to maps and models deposited at the EMDB and PDB, respectively, were published between 2000 and 2016, a period corresponding to the time axis of these graphs.

Figure 2. Liquid-state NMR studies provide 3D structures for small components or binders of large complexes analysed by cryoEM. (A) 3.5 Å cryoEM map of yeast 26S proteasome lid (EMDB 6479) with docked N-terminal (in orange; PDB 2MQW) and C-terminal (in red; PDB 2MRI) domain solution structures of Rpn9 (PDB ID of the final model: 3JCK). In the framed panel, two 3D structures of the N-terminal Rpn9 domain are superimposed: the model built from the cryoEM map (in light blue and displayed in rainbow colours below on the left) and the NMR structure (in orange, also displayed in rainbow colours below on the right). **(B)** The cofilin NMR solution structure (20 superimposed structures in rainbow colours; PDB 1Q8G) was fitted into the 9 Å cryoEM map of cofilin bound to actin filaments (docked cofilin structures in orange and red; EMDB 5354; PDB ID of the final model 3J0S). **(C)** The solution structure of the inhibitor Emi1 (20 superimposed structures in rainbow colours; PDB 2M6N) was fitted into the 3.6 Å resolution cryoEM reconstruction of APC/C (docked structure of the Emi1 fragment studied by NMR in orange and structures of Emi1 additional extended fragments in red) (EMDB 2924; PDB 4UI9).

Figure 3. Liquid- or solid-state NMR data are combined with cryoEM maps to provide models for filaments and needles. (A) Fitting of the NMR solution structure of the PB1 domain (from amino acid 1 to amino acid 122) from the autophagy receptor p62 (20 superimposed structures in rainbow colours; PDB 2KKC) into the 10.3 Å cryoEM reconstruction of PB1 filaments (EMDB 2937; PDB 4UF9). One PB1 subunit structure is shown in red and its directly interacting PB1 neighbours in yellow. The other PB1 structures are in orange. The arrow points to the C-terminus of a yellow subunit that interacts with the red subunit. **(B)** Fitting of the NMR solution structure of the pyrin domain of

human ASC (PDB 1UCP) into the 3.8 Å resolution cryoEM reconstruction of the ASC filaments (EMDB 5830, PDB 3J63). In the upper view, one pyrin domain is shown in red and the others are in orange. In the lower view, superimposition of the NMR solution structures of the ASC pyrin domain (in grey and green) with the pyrin structure fitted into the cryoEM reconstruction of the ASC filaments indicates that conformational changes occurred in loop α2-α3 and in helix α3 during filament assembly. **(C)** Hybrid structure of the *Shigella flexneri* type III secretion system needle obtained from solid-state NMR and EM data at 7.7 Å resolution (EMDB 5352; PDB 2MME). The solid state NMR structure determined in this work is shown in the map in orange/red. The structure of four subunits derived from this hybrid study is shown in rainbow style (N-terminus in blue and C-terminus in red) and compared to the structure proposed in a previous study based only a cryoEM map (EMDB 5352; PDB 3J0R).

Figure 4. Architecture of phage SPP1 connector and tail as deduced from a combined liquid-state NMR and EM study. (A) Solution structure of the head-completion protein gp16 from phage SPP1 (PDB 2KCA). **(B,C)** Flexible fitting of the NMR structure of gp16 into the cryoEM reconstruction of the head-to-tail interface of SPP1 in its closed state (EMDB 2993; PDB 5A20). Twelve gp16 molecules are present in each phage particle. The dashed arrow links the loop closing the connector channel in **(B)** and **(C).** In **(B)** is shown a subunit extracted from the modelled dodecamer, for comparison with **(A).** In **(C)** is shown the fitting of the 12 gp16 monomers into the corresponding cryoEM density. The protein structures are displayed in green excepted for a single subunit coloured in purple. **(D)** Flexible fitting of the head-completion proteins gp15 (in salmon; PDB 2KBZ) and gp16 (in green; PDB 2KCA) and the tail-completion protein gp17 (in orange; PDB 2LFP) into the cryoEM map of the head-to-tail interface of SPP1 in its closed state.

References

1. Levitt MH: *Spin Dynamics: Basics of Nuclear Magnetic Resonance* edn 2 edn. Chichester; 2008.
2. Brutscher B, Felli IC, Gil-Caballero S, Hosek T, Kummerle R, Piai A, Pierattelli R, Solyom Z: **NMR Methods for the Study of Instrinsically Disordered Proteins Structure, Dynamics, and Interactions: General Overview and Practical Guidelines**. *Adv Exp Med Biol* 2015, **870**:49-122.
3. Merk A, Bartesaghi A, Banerjee S, Falconieri V, Rao P, Davis MI, Pragani R, Boxer MB, Earl LA, Milne JLS, et al.: **Breaking Cryo-EM Resolution Barriers to Facilitate Drug Discovery**. *Cell* 2016, **165**:1698-1707.
4. Behrmann E, Loerke J, Budkevich TV, Yamamoto K, Schmidt A, Penczek PA, Vos MR, Burger J, Mielke T, Scheerer P, et al.: **Structural snapshots of actively translating human ribosomes**. *Cell* 2015, **161**:845-857.
5. Doerschuk PC, Gong Y, Xu N, Domitrovic T, Johnson JE: **Virus particle dynamics derived from CryoEM studies**. *Curr Opin Virol* 2016, **18**:57-63.
6. Subramaniam S, Kuhlbrandt W, Henderson R: **CryoEM at IUCrJ: a new era**. *IUCrJ* 2016, **3**:3-7.
7. Kuhlbrandt W: **Biochemistry. The resolution revolution**. *Science* 2014, **343**:1443-1444.
8. Vinothkumar KR, Zhu J, Hirst J: **Architecture of mammalian respiratory complex I**. *Nature* 2014, **515**:80-84.
9. Kostyuchenko VA, Lim EX, Zhang S, Fibriansah G, Ng TS, Ooi JS, Shi J, Lok SM: **Structure of the thermally stable Zika virus**. *Nature* 2016, **533**:425-428.
10. Sirohi D, Chen Z, Sun L, Klose T, Pierson TC, Rossmann MG, Kuhn RJ: **The 3.8 A resolution cryo-EM structure of Zika virus**. *Science* 2016, **352**:467-470.

11. Nguyen TH, Galej WP, Fica SM, Lin PC, Newman AJ, Nagai K: **CryoEM structures of two spliceosomal complexes: starter and dessert at the spliceosome feast**. *Curr Opin Struct Biol* 2016, **36**:48-57.
12. Zhao J, Benlekbir S, Rubinstein JL: **Electron cryomicroscopy observation of rotational states in a eukaryotic V-ATPase**. *Nature* 2015, **521**:241-245.
13. Nogales E, Scheres SH: **Cryo-EM: A Unique Tool for the Visualization of Macromolecular Complexity**. *Mol Cell* 2015, **58**:677-689.
14. Lengyel J, Hnath E, Storms M, Wohlfarth T: **Towards an integrative structural biology approach: combining Cryo-TEM, X-ray crystallography, and NMR**. *J Struct Funct Genomics* 2014, **15**:117-124.
15. Gong Z, Schwieters CD, Tang C: **Conjoined use of EM and NMR in RNA structure refinement**. *PLoS One* 2015, **10**:e0120445.
16. Mueller F, Sommer I, Baranov P, Matadeen R, Stoldt M, Wohnert J, Gorlach M, van Heel M, Brimacombe R: **The 3D arrangement of the 23 S and 5 S rRNA in the Escherichia coli 50 S ribosomal subunit based on a cryo-electron microscopic reconstruction at 7.5 A resolution**. *J Mol Biol* 2000, **298**:35-59.
17. Agrawal RK, Linde J, Sengupta J, Nierhaus KH, Frank J: **Localization of L11 protein on the ribosome and elucidation of its involvement in EF-G-dependent translocation**. *J Mol Biol* 2001, **311**:777-787.
18. Valle M, Zavialov A, Li W, Stagg SM, Sengupta J, Nielsen RC, Nissen P, Harvey SC, Ehrenberg M, Frank J: **Incorporation of aminoacyl-tRNA into the ribosome as seen by cryo-electron microscopy**. *Nat Struct Biol* 2003, **10**:899-906.
19. Boehringer D, Thermann R, Ostareck-Lederer A, Lewis JD, Stark H: **Structure of the hepatitis C virus IRES bound to the human 80S ribosome: remodeling of the HCV IRES**. *Structure* 2005, **13**:1695-1706.
20. Yamamoto H, Collier M, Loerke J, Ismer J, Schmidt A, Hilal T, Sprink T, Yamamoto K, Mielke T, Burger J, et al.: **Molecular architecture of the ribosome-bound Hepatitis C Virus internal ribosomal entry site RNA**. *EMBO J* 2015, **34**:3042-3058.
21. Jiang J, Chan H, Cash DD, Miracco EJ, Ogorzalek Loo RR, Upton HE, Cascio D, O'Brien Johnson R, Collins K, Loo JA, et al.: **Structure of Tetrahymena telomerase reveals previously unknown subunits, functions, and interactions**. *Science* 2015, **350**:aab4070.
22. Fernandez-Leiro R, Conrad J, Scheres SH, Lamers MH: **cryo-EM structures of the replicative DNA polymerase reveal its dynamic interactions with the DNA sliding clamp, exonuclease and**. *Elife* 2015, **4**.
23. Hu Y, Wu Y, Li Q, Zhang W, Jin C: **Solution structure of yeast Rpn9: insights into proteasome lid assembly**. *J Biol Chem* 2015, **290**:6878-6889.
24. Dambacher CM, Worden EJ, Herzik MA, Martin A, Lander GC: **Atomic structure of the 26S proteasome lid reveals the mechanism of deubiquitinase inhibition**. *Elife* 2016, **5**:e13027.
25. Fotin A, Cheng Y, Grigorieff N, Walz T, Harrison SC, Kirchhausen T: **Structure of an auxilin-bound clathrin coat and its implications for the mechanism of uncoating**. *Nature* 2004, **432**:649-653.
26. Fourniol FJ, Sindelar CV, Amigues B, Clare DK, Thomas G, Perderiset M, Francis F, Houdusse A, Moores CA: **Template-free 13-protofilament microtubule-MAP assembly visualized at 8 A resolution**. *J Cell Biol* 2010, **191**:463-470.
27. Galkin VE, Orlova A, Kudryashov DS, Solodukhin A, Reisler E, Schroder GF, Egelman EH: **Remodeling of actin filaments by ADF/cofilin proteins**. *Proc Natl Acad Sci U S A* 2011, **108**:20568-20572.
28. Frye JJ, Brown NG, Petzold G, Watson ER, Grace CR, Nourse A, Jarvis MA, Kriwacki RW, Peters JM, Stark H, et al.: **Electron microscopy structure of human APC/C(CDH1)-EMI1 reveals multimodal mechanism of E3 ligase shutdown**. *Nat Struct Mol Biol* 2013, **20**:827-835.
29. Chang L, Zhang Z, Yang J, McLaughlin SH, Barford D: **Atomic structure of the APC/C and its mechanism of protein ubiquitination**. *Nature* 2015, **522**:450-454.

30. Ciuffa R, Lamark T, Tarafder AK, Guesdon A, Rybina S, Hagen WJ, Johansen T, Sachse C: **The selective autophagy receptor p62 forms a flexible filamentous helical scaffold**. *Cell Rep* 2015, **11**:748-758.
31. Lu A, Magupalli VG, Ruan J, Yin Q, Atianand MK, Vos MR, Schroder GF, Fitzgerald KA, Wu H, Egelman EH: **Unified polymerization mechanism for the assembly of ASC-dependent inflammasomes**. *Cell* 2014, **156**:1193-1206.
32. Demers JP, Habenstein B, Loquet A, Kumar Vasa S, Giller K, Becker S, Baker D, Lange A, Sgourakis NG: **High-resolution structure of the Shigella type-III secretion needle by solid-state NMR and cryo-electron microscopy**. *Nat Commun* 2014, **5**:4976.
33. Fujii T, Cheung M, Blanco A, Kato T, Blocker AJ, Namba K: **Structure of a type III secretion needle at 7-A resolution provides insights into its assembly and signaling mechanisms**. *Proc Natl Acad Sci U S A* 2012, **109**:4461-4466.
34. Loquet A, Sgourakis NG, Gupta R, Giller K, Riedel D, Goosmann C, Griesinger C, Kolbe M, Baker D, Becker S, et al.: **Atomic model of the type III secretion system needle**. *Nature* 2012, **486**:276-279.
35. Sborgi L, Ravotti F, Dandey VP, Dick MS, Mazur A, Reckel S, Chami M, Scherer S, Huber M, Bockmann A, et al.: **Structure and assembly of the mouse ASC inflammasome by combined NMR spectroscopy and cryo-electron microscopy**. *Proc Natl Acad Sci U S A* 2015, **112**:13237-13242.
36. Karamanos TK, Kalverda AP, Thompson GS, Radford SE: **Mechanisms of amyloid formation revealed by solution NMR**. *Prog Nucl Magn Reson Spectrosc* 2015, **88-89**:86-104.
37. Fitzpatrick AW, Debelouchina GT, Bayro MJ, Clare DK, Caporini MA, Bajaj VS, Jaroniec CP, Wang L, Ladizhansky V, Muller SA, et al.: **Atomic structure and hierarchical assembly of a cross-beta amyloid fibril**. *Proc Natl Acad Sci U S A* 2013, **110**:5468-5473.
38. Zinkevich T, Chevelkov V, Reif B, Saalwachter K, Krushelnitsky A: **Internal protein dynamics on ps to mus timescales as studied by multi-frequency (15)N solid-state NMR relaxation**. *J Biomol NMR* 2013, **57**:219-235.
39. Scheidt HA, Morgado I, Rothemund S, Huster D: **Dynamics of amyloid beta fibrils revealed by solid-state NMR**. *J Biol Chem* 2012, **287**:2017-2021.
40. Smith AA, Testori E, Cadalbert R, Meier BH, Ernst M: **Characterization of fibril dynamics on three timescales by solid-state NMR**. *J Biomol NMR* 2016, **65**:171-191.
41. Orlova EV, Gowen B, Droge A, Stiege A, Weise F, Lurz R, van Heel M, Tavares P: **Structure of a viral DNA gatekeeper at 10 A resolution by cryo-electron microscopy**. *EMBO J* 2003, **22**:1255-1262.
42. Chaban Y, Lurz R, Brasiles S, Cornilleau C, Karreman M, Zinn-Justin S, Tavares P, Orlova EV: **Structural rearrangements in the phage head-to-tail interface during assembly and infection**. *Proc Natl Acad Sci U S A* 2015, **112**:7009-7014.
43. Lebedev AA, Krause MH, Isidro AL, Vagin AA, Orlova EV, Turner J, Dodson EJ, Tavares P, Antson AA: **Structural framework for DNA translocation via the viral portal protein**. *EMBO J* 2007, **26**:1984-1994.
44. Lhuillier S, Gallopin M, Gilquin B, Brasiles S, Lancelot N, Letellier G, Gilles M, Dethan G, Orlova EV, Couprie J, et al.: **Structure of bacteriophage SPP1 head-to-tail connection reveals mechanism for viral DNA gating**. *Proc Natl Acad Sci U S A* 2009, **106**:8507-8512.
45. Chagot B, Auzat I, Gallopin M, Petitpas I, Gilquin B, Tavares P, Zinn-Justin S: **Solution structure of gp17 from the Siphoviridae bacteriophage SPP1: insights into its role in virion assembly**. *Proteins* 2012, **80**:319-326.
46. Rizzo AA, Suhanovsky MM, Baker ML, Fraser LC, Jones LM, Rempel DL, Gross ML, Chiu W, Alexandrescu AT, Teschke CM: **Multiple functional roles of the accessory I-domain of bacteriophage P22 coat protein revealed by NMR structure and CryoEM modeling**. *Structure* 2014, **22**:830-841.

47. Byeon IJ, Meng X, Jung J, Zhao G, Yang R, Ahn J, Shi J, Concel J, Aiken C, Zhang P, et al.: **Structural convergence between Cryo-EM and NMR reveals intersubunit interactions critical for HIV-1 capsid function**. *Cell* 2009, **139**:780-790.
48. Zhao G, Perilla JR, Yufenyuy EL, Meng X, Chen B, Ning J, Ahn J, Gronenborn AM, Schulten K, Aiken C, et al.: **Mature HIV-1 capsid structure by cryo-electron microscopy and all-atom molecular dynamics**. *Nature* 2013, **497**:643-646.
49. Bharat TA, Davey NE, Ulbrich P, Riches JD, de Marco A, Rumlova M, Sachse C, Ruml T, Briggs JA: **Structure of the immature retroviral capsid at 8 A resolution by cryo-electron microscopy**. *Nature* 2012, **487**:385-389.
50. Macek P, Chmelik J, Krizova I, Kaderavek P, Padrta P, Zidek L, Wildova M, Hadravova R, Chaloupkova R, Pichova I, et al.: **NMR structure of the N-terminal domain of capsid protein from the mason-pfizer monkey virus**. *J Mol Biol* 2009, **392**:100-114.
51. Liu C, Perilla JR, Ning J, Lu M, Hou G, Ramalho R, Himes BA, Zhao G, Bedwell GJ, Byeon IJ, et al.: **Cyclophilin A stabilizes the HIV-1 capsid through a novel non-canonical binding site**. *Nat Commun* 2016, **7**:10714.
52. Huang R, Ripstein ZA, Augustyniak R, Lazniewski M, Ginalski K, Kay LE, Rubinstein JL: **Unfolding the mechanism of the AAA+ unfoldase VAT by a combined cryo-EM, solution NMR study**. *Proc Natl Acad Sci U S A* 2016, **113**:E4190-4199.

Selected references

** 21. Jiang J, Chan H, Cash DD, Miracco EJ, Ogorzalek Loo RR, Upton HE, Cascio D, O'Brien Johnson R, Collins K, Loo JA, et al.: **Structure of Tetrahymena telomerase reveals previously unknown subunits, functions, and interactions**. *Science* 2015, **350**:aab4070.

The authors reported the first pseudoatomic model of a telomerase complex, calculated from mass spectrometry, negative-staining EM, cryoEM, X-ray crystallography and NMR data. This complex contains the integral telomerase RNA (TER), the telomerase reverse transcriptase (TERT) and several additional proteins including a telomeric G-strand binding protein. The NMR structure of the TER pseudoknot, as well as the X-ray structures of two of the additional proteins, were determined. Altogether, this study revealed the path of TER on TERT and suggested an exit path for the telomeric repeat DNA.

* 28. Frye JJ, Brown NG, Petzold G, Watson ER, Grace CR, Nourse A, Jarvis MA, Kriwacki RW, Peters JM, Stark H, et al.: **Electron microscopy structure of human APC/C(CDH1)-EMI1 reveals multimodal mechanism of E3 ligase shutdown**. *Nat Struct Mol Biol* 2013, **20**:827-835.

This study represents one of the few examples in which NMR is used to identify the disordered fragments in a free monomeric ligand and cryoEM is used to position these fragments in the 3D structure of the ligand bound to a complex. Here chimera of the ligand were produced, in which a globular domain is inserted into each disordered fragment, and observation of these chimera by cryoEM identified the engineered fragments in the complex.

** 32. Demers JP, Habenstein B, Loquet A, Kumar Vasa S, Giller K, Becker S, Baker D, Lange A, Sgourakis NG: **High-resolution structure of the Shigella type-III secretion needle by solid-state NMR and cryo-electron microscopy**. *Nat Commun* 2014, **5**:4976.

This article showed for the first time how solid-state NMR and cryoEM data can be integrated in order to determine the 3D structure of a protein oligomer. The structure was cross-validated using an independent set of NMR constraints and STEM measurements.

** 37. Fitzpatrick AW, Debelouchina GT, Bayro MJ, Clare DK, Caporini MA, Bajaj VS, Jaroniec CP, Wang L, Ladizhansky V, Muller SA, et al.: **Atomic structure and hierarchical assembly of a cross-beta amyloid fibril**. *Proc Natl Acad Sci U S A* 2013, **110**:5468-5473.

The authors used a panel of peptide labeling schemes and solid-state NMR experiments, together with single-particle and helical cryoEM approaches, to determine the overall structure of three polymorphs formed by a 11-residue peptide of transthyretin. Description of the

subsets of fibril populations was further supported by X-ray diffraction, scanning transmission electron microscopy and atomic force microscopy measurements.

** 42. Chaban Y, Lurz R, Brasiles S, Cornilleau C, Karreman M, Zinn-Justin S, Tavares P, Orlova EV: **Structural rearrangements in the phage head-to-tail interface during assembly and infection**. *Proc Natl Acad Sci U S A* 2015, **112**:7009-7014.

The authors revealed mechanisms for phage particle assembly and function from the docking of several X-ray and NMR structures into the EM maps of the phage head-to-tail connector and tail studied before and after DNA ejection. The phage proteins exhibit conformational disorder before assembly into the phage particles. Conformational changes are observed between the different phage particle functional states. These are essential for phage capacity to infect a bacteria.

* 47. Byeon IJ, Meng X, Jung J, Zhao G, Yang R, Ahn J, Shi J, Concel J, Aiken C, Zhang P, et al.: **Structural convergence between Cryo-EM and NMR reveals intersubunit interactions critical for HIV-1 capsid function**. *Cell* 2009, **139**:780-790.

The authors revealed the relative positioning of the HIV-1 capsid protein domains within a tubular assembly of capsid proteins. They showed that the NMR structure of the C-terminal domain dimer fits well into the EM density map, which is not the case of previous X-ray structures. They confirmed the importance of the identified protein-protein interfaces by mutagenesis.

** 52. Huang R, Ripstein ZA, Augustyniak R, Lazniewski M, Ginalski K, Kay LE, Rubinstein JL: **Unfolding the mechanism of the AAA+ unfoldase VAT by a combined cryo-EM, solution NMR study**. *Proc Natl Acad Sci U S A* 2016, **113**:E4190-4199.

This article illustrates how cryoEM and liquid-state NMR can be combined to describe a population distribution of conformers in a large molecular machine. Here key features of the cryoEM model are validated using biochemical as well as methyl-transverse relaxation optimized spectroscopy NMR experiments.

A

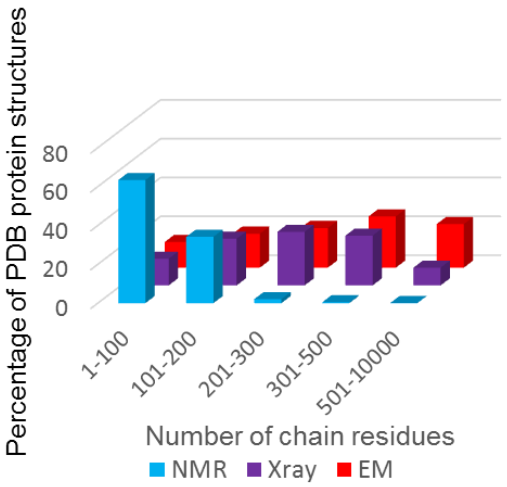

B

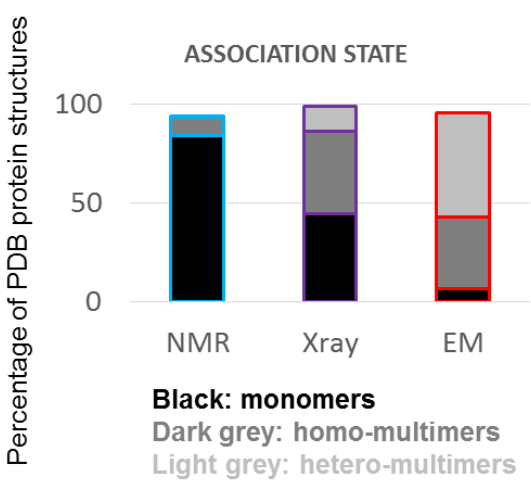

C

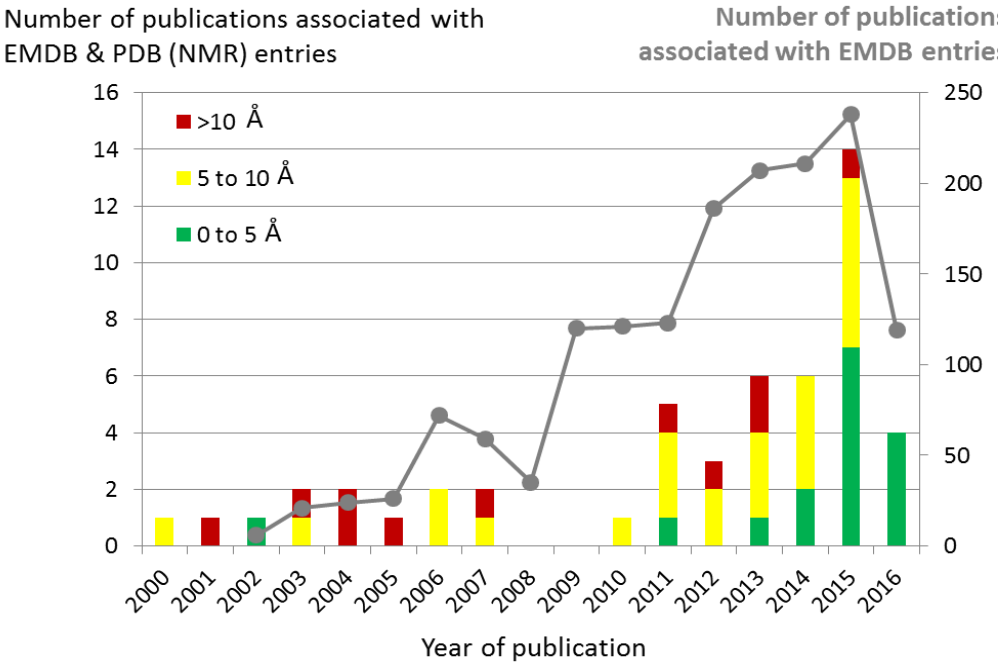

D

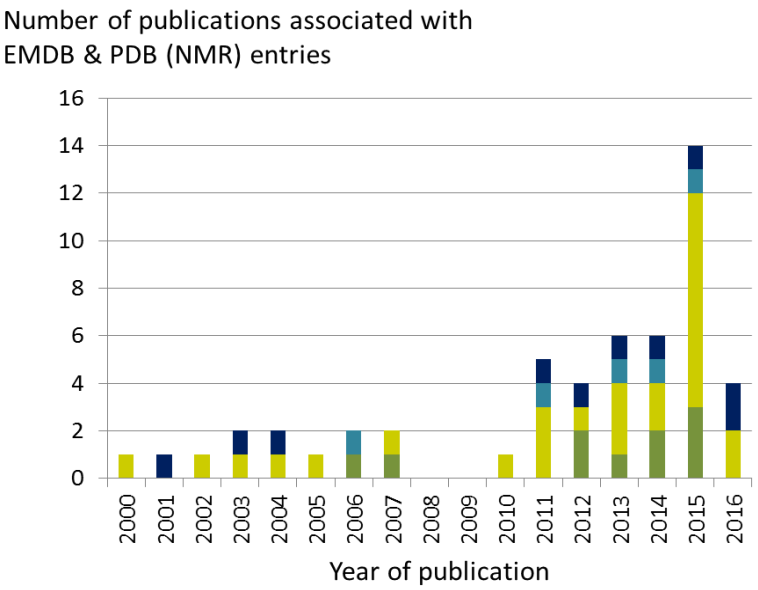

Fitting into a cryoEM map of homology models built from NMR structures or validation of the interfaces by NMR

Model calculated from EM and solid-state NMR data (ex: figure 3C)

Fitting into a cryoEM map of protein and RNA liquid-state NMR structures that contribute to part of the model (ex: figure 2)

Model built from EM and liquid-state NMR data (ex: figure 3A,B)

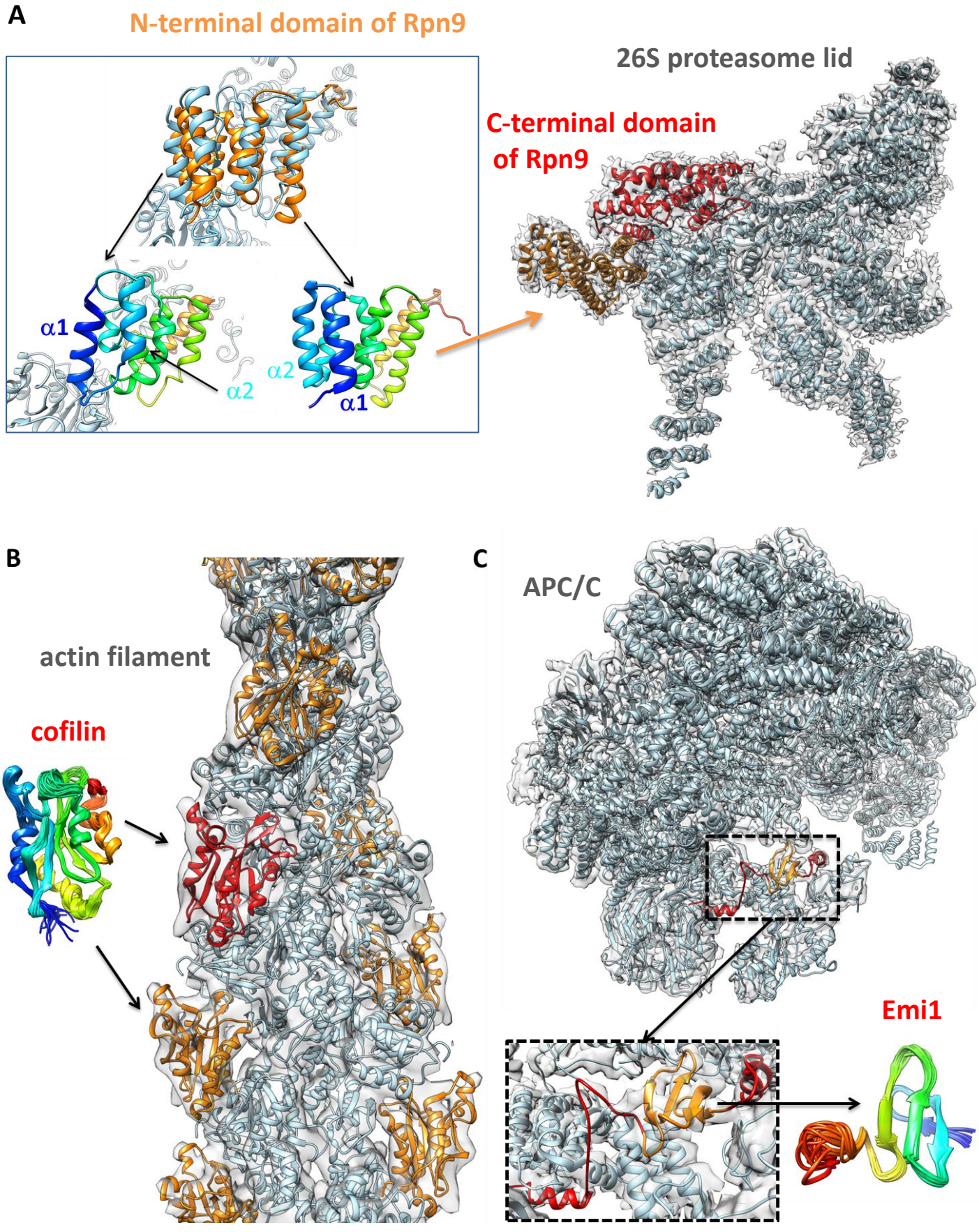
A
N-terminal domain of Rpn9
α1
α2
α2
α1
26S proteasome lid
C-terminal domain
of Rpn9
B
actin filament
cofilin
C
APC/C
Emi1

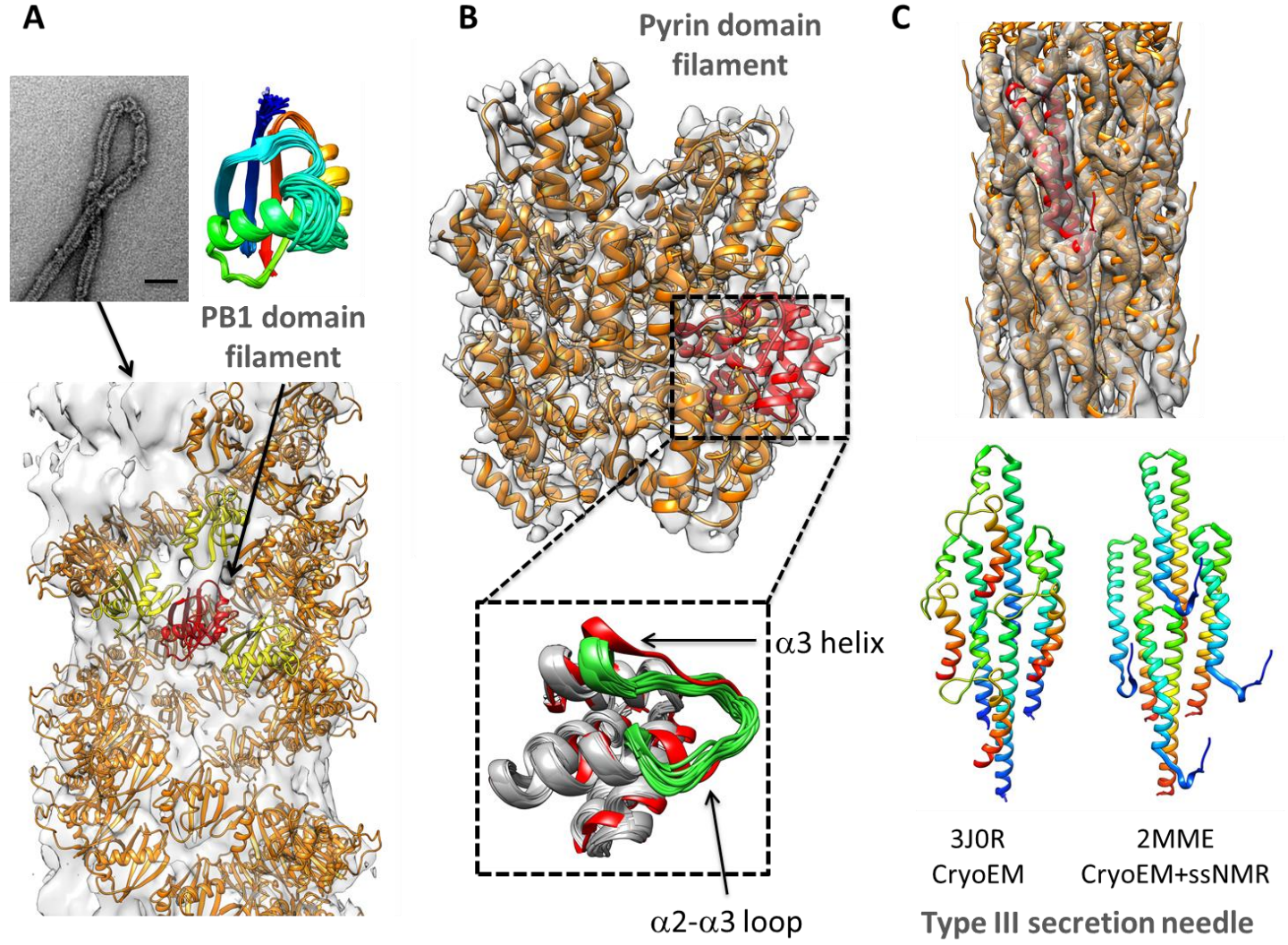
A
PB1 domain filament
B
Pyrin domain filament
α3 helix
α2-α3 loop
C
3J0R
CryoEM
2MME
CryoEM+ssNMR
Type III secretion needle

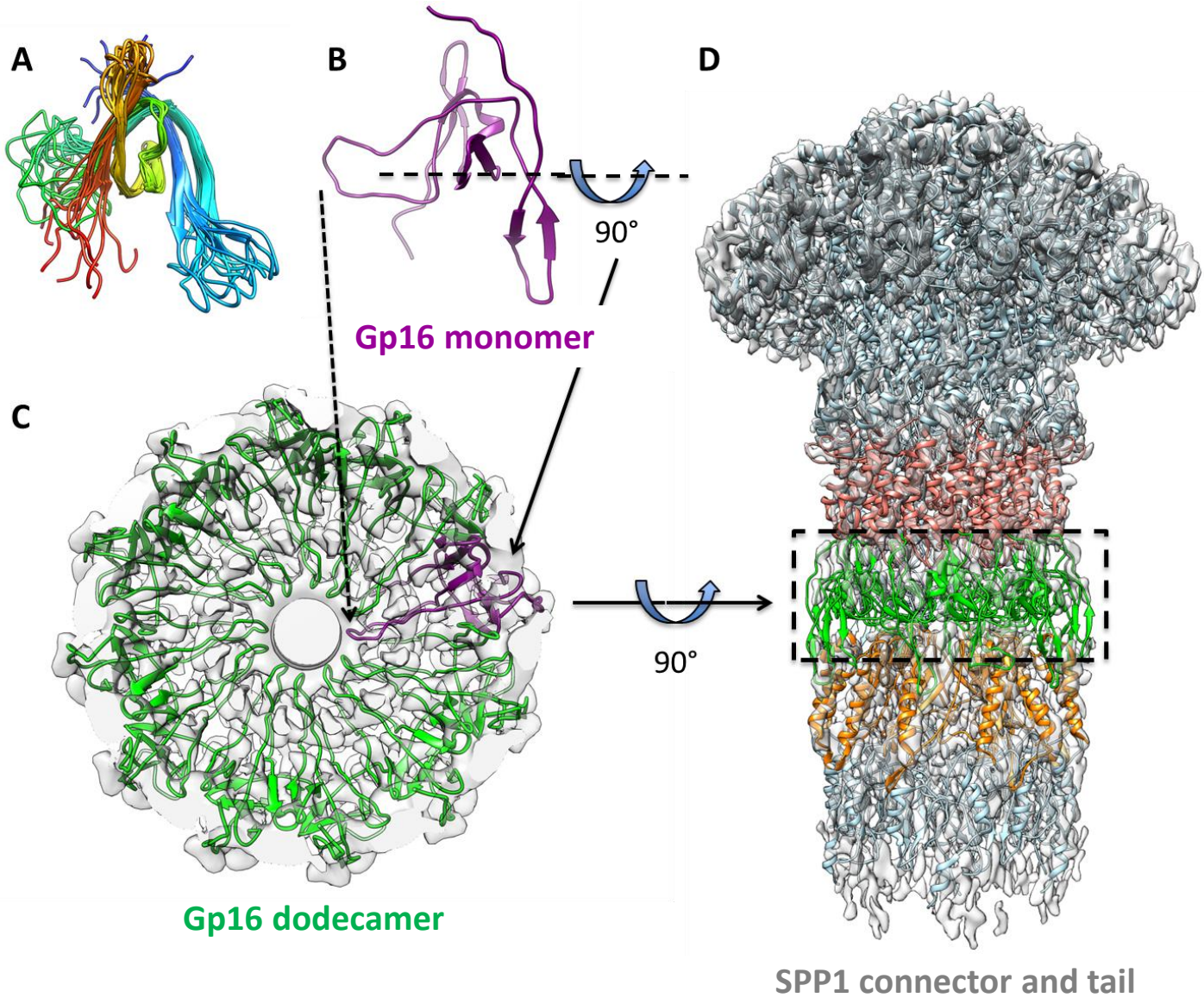
A
B
D
90°
Gp16 monomer
C
90°
Gp16 dodecamer
SPP1 connector and tail